

# DECOMPOSITION OF AIRBORNE LASER SCANNING WAVEFORM DATA BASED ON EM ALGORITHM

Qi Li\*

School of Remote Sensing and Information Engineering, Wuhan University.129 Luoyu Road, Wuhan 430079

**KEY WORDS:** LIDAR, Waveform-digitizing, Analysis of waveform, Filter, Smooth, Gaussian decomposition, DSM, DTM, Forest structure

## ABSTRACT:

Data storage capacity and high processing speed available today has made it possible to digitally sample and store the entire reflected waveform of Small-Footprint Airborne Lidar (light detection and ranging), instead of only extracting the discrete coordinates which form the so-called point clouds. One of the most important advantages from waveforms data is that it gives the user the chance to extract three-dimensional coordinates by himself in the post-processing. Decomposition return waveform is a key step during analyzing waveform data. Conventional algorithm to decompose is maximum and centre of gravity, or simply by using the thresholding method provided by equipment vendor. Both show lack of high accuracy. In this paper, an improved Expectation Maximum (EM) algorithm is adopted to extract peak location and pulse width from raw waveform data, proving it is a reliable and high accurate decomposition algorithm. Moreover, the high-quality point-cloud data could be obtained which provides high-quality resources for DSM(Digital Surface Model) and DTM (Digital Terrain Model) production. Derived forest biophysical parameters, such as vegetation height and crown volume are able to describe the horizontal and vertical forest canopy structure.

## 1. INTRODUCTION

In the last ten years, airborne laser scanning is a rapidly growing technology which has initially been conceived for topographic mapping. Airborne laser scanners employ, with few exceptions, pulsed lasers that repetitively emit short infrared pulses towards the Earth's surface. Some of the energy is scattered back to the sensor where it is measured with an optical receiver. A timer measures the traveling time of the pulse from the laser scanner to the Earth's surface and back, the integration of laser with GPS and INS for position and orientation determination. Nowadays, ALS is used routinely for topographic mapping and is considered to hold a large potential in a range of other applications such as forestry, 3D city modeling or power line detection.

Development of airborne laser scanning goes back to the 1970s and 1980s. The first commercially available airborne laser scanners recorded the time of one backscattered pulse. The recording of only one pulse is sufficient if there is only one target within the laser footprint. State-of-the-art commercial laser scanners typically measure first and last pulse; some are able to measure up to five pulses. In order to derive digital terrain models (DTMs), laser pulses reflected by the ground surface must be distinguished from non-terrain points. This task can be achieved using various filtering techniques that classify the point cloud into terrain and off-terrain points just based on the spatial relationship of the 3D data. For many applications, this has been deemed the suitable form of output. However, the user has no way of knowing how the electronics of his LIDAR system actually determine the location of the returns they report, nor of any distortions of the pulse shape that receiver electronics or surface structures may have imposed upon the pulse echo. LIDAR system manufacturers are tight-lipped about the pulse detection methods their systems employ. However, as Wagner et al. (2004) point out the choice of pulse detection methods has significant impact on accuracy, and in practice causes a number of effects that reduce the quality of the measurements, like amplitude dependant range walk, slope dependency of range,

signal ringing causing outlier measurements below the terrain level, etc. In addition, with mere range output much of the informational content about structured surfaces is lost.

The solution is to digitally sample and store the entire echo waveform of reflected laser pulses. Digitizing and recording the complete backscattered waveform during the acquisition for later post-processing has the advantages that algorithms can be adjusted to tasks, intermediate results are respected, and neighborhood relations of pulses can be considered. The technical feasibility has been demonstrated by large-footprint airborne systems developed by NASA in the 1990s, namely the Scanning Lidar Imager of Canopies by Echo Recover (SLICER) and the Laser Vegetation Imaging Sensor (LVIS). Recently, three commercial airborne systems have become available, such as Figure 1, namely the RIEGL LMS-Q560, Toposys FalconIII, Leica ALS-II, Optech ALTM 3100E.

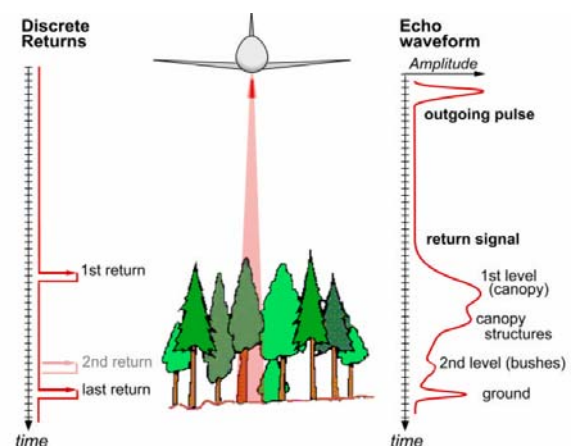


Fig.1 waveform Digitization

An approach based on unsupervised learning is presented where a mixture of Gaussian distributions are fitted to the waveforms

\* Email:qli\_rs@yahoo.com.cn

to detect and parameterize the peaks. This approach uses the Expectation Maximization (EM) algorithm (Dempster et al., 1977). A detection algorithm based on the expectation-maximization (EM) algorithm is used to estimate the number of echo pulses of the waveforms.

## 2. GENERATION AND DECOMPOSITION OF WAVEFORM

The power entering the receiver is

$$P_r(t) = \sum_{i=1}^N \frac{D_r^2}{4\pi R_i^4 \beta_i^2} P_t(t) * \sigma_i'(t) * \Gamma(t)$$

$N$  is distinct targets within the travel path of the laser pulse,  $P_t(t)$  is the transmitted power;  $P_r(t)$  is the received power;  $D_r$  is the aperture diameter of the receiver optics;  $R_i$  is the range between scanner and object  $i$ ;  $\sigma_i'(t)$  is the so-called backscatter cross-section;  $\Gamma(t)$  is the receiver impulse function;  $*$  is the convolution operator. In practice,  $P_t(t)$  and  $\Gamma(t)$  cannot be easily determined independently. Therefore it is advantageous to rewrite the convolution term by making use of the commutative property of the convolution operator:

$$P_t(t) * \sigma_i'(t) * \Gamma(t) = P_t(t) * \Gamma(t) * \sigma_i'(t)$$

where we introduce the system waveform  $S(t)$  of the laser scanner, defined as the convolution of the transmitted pulse and the receiver response function. It can be measured experimentally and is shown in Figure. 2 for the Riegl LMS-Q560. It can be seen that it is well described by a Gaussian function:

$$S(t) = \hat{S} e^{-\frac{t^2}{2s_s^2}}$$

$\hat{S}$  is the amplitude,  $s_s$  is the standard deviation. In order to come to an analytical waveform solution, let us assume that the scattering properties of a cluster of scatterers can be described by a Gaussian function:

$$\sigma_i'(t) = \hat{\sigma}_i e^{-\frac{(t-t_i)^2}{2s_i^2}}, \hat{\sigma}_i \text{ is the amplitude and } s_i \text{ the standard deviation.}$$

The convolution of two Gaussian curves gives again a Gaussian function, so that we obtain:

$$P_r(t) = \sum_{i=1}^N \hat{P}_i e^{-\frac{(t-t_i)^2}{2s_{p,i}^2}}$$

$$s_{p,i} = \sqrt{s_s^2 + s_i^2}, \hat{P}_i = \frac{D_r^2}{4\pi R_i^4 \beta_i^2} \hat{S} \hat{\sigma}_i \frac{s_s}{s_{p,i}}$$

Thus it can be seen the return waveforms are made up by Gaussians has proven to be a fairly good approximation.

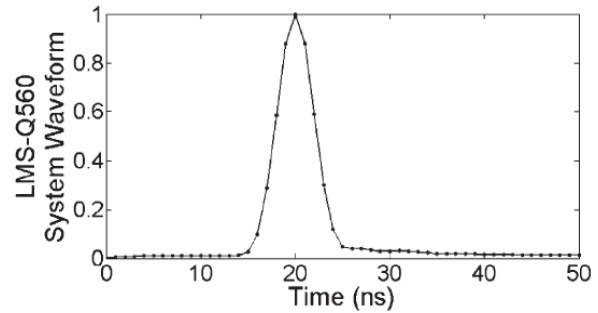


Fig.2 System waveform of RIEGL LM-5600

## 3. ALGORITHM OF DECOMPOSING WANEFORM

To consistently geolocate the desired reflecting surface, for example, the underlying ground surface in vegetated regions, we need to be able to precisely identify the corresponding reflection within the waveform. Existing waveform processing methods generally do not take into account surface type nor its effect on the shape of the return laser pulse, and thus do not provide a consistent ranging point to a reflecting surface during data processing. These methods include finding the location of the peak amplitude within the waveform or the location of the centroid of the return waveform. Experiments illustrate that there is no such thing as a single best detector, rather the relative performance of the detectors depends on factors such as the characteristics of the effective scattering cross section, object distance and noise level.

Thus, we propose to decompose a return waveform into components, the sum of which can be used to approximate the waveform and the locations of which can be used to improve the geolocation accuracy of the laser altimeter. We will assume that each mode represents the reflected distribution of laser energy from a reflecting surface within the footprint, and that the location of each mode can be used to geolocate the reflecting surface of interest in the vertical direction. Gaussian decomposition presents us with one possible model of the reflections contained in a complex, multi-modal waveform.

As a first approximation we will assume that the laser output pulse shape or impulse response (i.e., the shape of the outgoing laser pulse after passing through the full detector and digitizer chain) is Gaussian. We further assume that the returning laser pulse is composed of a series of potentially-overlapping reflections similar in shape to the impulse response (i.e., in this case by a series of Gaussian-shaped reflections). As was shown in the theory part of the paper, the implicit assumption of Gaussian decomposition is that the cross-section profile can be represented by a series of Gaussian functions.

It is of interest to extract more than the first and the last echo from each waveform. Also, the width of the echoes is of interest. A detection algorithm based on the improved expectation-maximization (EM) algorithm is used to estimate the number of echo pulses of the waveforms. The algorithm also outputs the width of the echo pulses. Unsupervised learning is a method of machine learning where a model is fitted to observations. An important part of the unsupervised learning problem is determining the number of components or classes which best describe the data.

Unsupervised learning will be used in this thesis to detect echo pulses. This is done by fitting Gaussians to the waveforms. It will be assumed that the waveforms were generated from a distribution which is the sum of simpler distributions. That is, the samples of the waveforms are assumed to arise from the following distribution.

$$f(x) = \sum_{j=1}^k p_j \times f_j(x)$$

$$f_j(x) \in N(\mu_j, \sigma_j^2)$$

Where  $k$  is the number of Gaussians,  $f_j(x)$  is the Gaussian probability density function,  $p_j$  is the relative weight of  $f_j(x)$ ,  $\mu_j$  is the expected value and  $\sigma_j$  is the standard deviation of the fitted Gaussians.

The EM algorithm, which will be used to fit the Gaussians to the waveforms, is a widely used approach in learning the presence of unobserved variables. Original formula of EM algorithm:

$$Q_{ij} = \frac{p_j f_j(x_i)}{\sum_{j=1}^k p_j f_j(x_i)} \quad (1)$$

$$p_j = \frac{\sum_{i=1}^n Q_{ij}}{n} \quad (2)$$

$$\mu_j = \frac{\sum_{i=1}^n Q_{ij} i}{p_j \times n} \quad (3)$$

$$\sigma_j = \sqrt{\frac{\sum_{i=1}^n Q_{ij} (i - \mu_j)^2}{p_j \times n}} \quad (4)$$

$Q_{ij}$  is the probability that sample  $i$  belongs to component  $j$  and  $k$  is the number of components that are fitted to the waveforms. For each component  $j$ , the mean value  $\mu_j$  and standard deviation  $\sigma_j$  are estimated. The mean value  $\mu_j$  will be used as the position of the echo and the standard deviation  $\sigma_j$  as the width of the echo. The likelihood estimates for  $\mu_j$  and  $\sigma_j$  are found by iterating through formula (1)-(4). The algorithm needs to be initialized with start values.

In the estimation step of the EM algorithm, the expected value of each hidden variable is calculated assuming that the current hypothesis holds. In the maximization step (2)-(4), a new maximum likelihood hypothesis is calculated assuming that the value taken on by each hidden variable is its expected value calculated in the estimation step. The hypothesis is replaced by the new hypothesis and a new iteration is made. However, original formula of EM algorithm does not take into account the intensity of sample  $i$ . consequence of the improved EM algorithm:

Formula (2) insert in formula (3)-(4):

$$\mu_j = \frac{\sum_{i=1}^n Q_{ij} i}{\sum_{i=1}^n Q_{ij}} = \frac{n \times \sum_{i=1}^n Q_{ij} i}{\sum_{i=1}^n Q_{ij} \times n} = \frac{\sum_{i=1}^n Q_{ij} i}{\sum_{i=1}^n Q_{ij}} \quad (5)$$

$$\sigma_j = \sqrt{\frac{\sum_{i=1}^n Q_{ij} (i - \mu_j)^2}{n \times p_j}} = \sqrt{\frac{n \times \sum_{i=1}^n Q_{ij} (i - \mu_j)^2}{\sum_{i=1}^n Q_{ij} \times n}} = \sqrt{\frac{\sum_{i=1}^n Q_{ij} (i - \mu_j)^2}{\sum_{i=1}^n Q_{ij}}} \quad (6)$$

Now, intensity  $N_i$  insert in numerator and denominator:

$$\mu_j = \frac{\sum_{i=1}^n N_i Q_{ij} i}{\sum_{i=1}^n N_i Q_{ij}} \quad (7)$$

$$\sigma_j = \sqrt{\frac{\sum_{i=1}^n N_i Q_{ij} (i - \mu_j)^2}{\sum_{i=1}^n N_i Q_{ij}}} \quad (8)$$

Now, formula (7)-(8) revert to form of EM algorithm:

$$Q_{ij} = \frac{p_j f_j(i)}{\sum_{j=1}^k p_j f_j(i)} \quad (9)$$

$$p_j = \frac{\sum_{i=1}^n N_i Q_{ij}}{n \times \sum_{i=1}^n N_i} \quad (10)$$

$$\mu_j = \frac{\sum_{i=1}^n N_i Q_{ij} i}{n \times p_j \times \sum_{i=1}^n N_i} \quad (11)$$

$$\sigma_j = \sqrt{\frac{\sum_{i=1}^n N_i Q_{ij} (i - \mu_j)^2}{n \times p_j \times \sum_{i=1}^n N_i}} \quad (12)$$

$S$  is the number of samples in the waveform and  $N_i$  is the intensity for sample  $i$ .

## 4. EXPERIMENTS AND DISCUSSION

### 4.1 SLICER

The SLICER .dat data files are derived from the standard Laser Altimeter Processing Facility .geo files which include geolocation results and instrument data. The inclination and azimuth of the transmit pulse are also derived from the .geo roll, pitch and yaw data, simplifying correction for waveform slant range distances. The diameter of each laser footprint, based on an approximate laser divergence and the ranging distance, is also provided.

#### 4.1.1 Pre-processing

Figure 4 and Figure 5, The waveforms have to be thresholded to remove noise before the EM algorithm is applied. The threshold is derived on a per shot basis by establishing the mean background noise occurring in the waveform record, the last 5% of the waveform record is used to calculate threshold  $\sigma_{noise}$ .

All samples of the waveform below the threshold  $\sigma_{noise}$  are then set to zero.

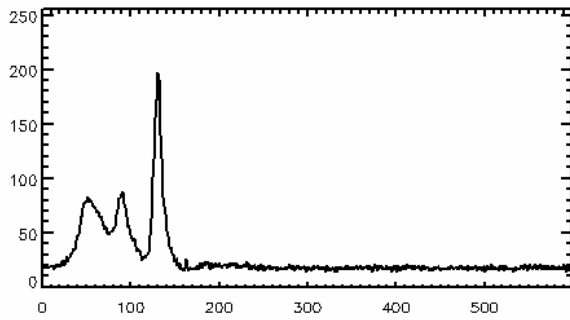


Fig.4 Unprocessed waveform

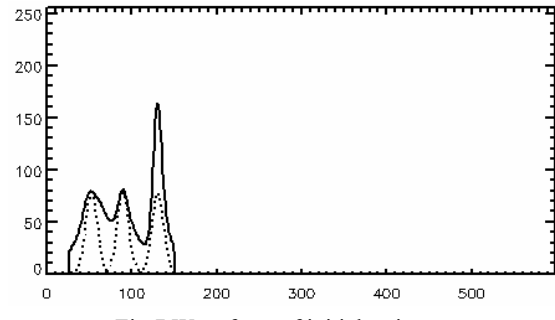


Fig.7 Waveform of initial estimates

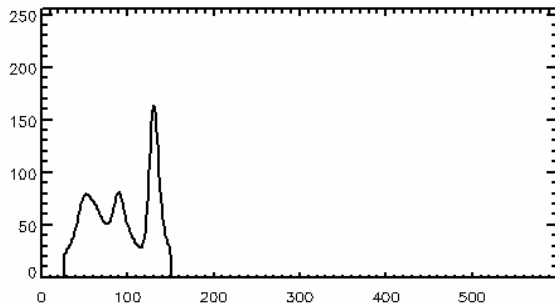


Fig.5 Pre-processed waveform

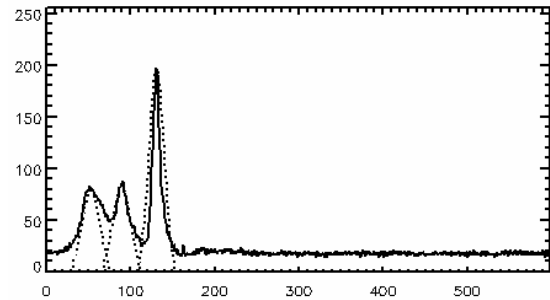


Fig.8 processed waveform

#### 4.1.2 Start values

The correctness of the initial values of  $\mu_j$ ,  $p_j$  and  $\sigma_j$  is important for the EM algorithm to generate a good estimate. The initial value for  $\mu_j$ , is found by smoothing the pre-processed signal and First derivative of waveform, Figure 6. The initial values for  $\mu_j$  are placed in the positions of the local maxima. If there are more components to estimate than the number of local maxima, the extra start values are put in the position of the local maxima with the greatest number of consecutive nonzero samples. Figure 7 illustrates a waveform (solid) and its initial estimates (dashed). The start values for  $p_j$  are set so that all components have an equal weight and  $\sigma_j$  is set to 7.

Waveform (solid) and Three gauss components(dashed) have been estimated from the waveform in Figure 8. The estimated parameter :  $\mu_1=54$ ,  $\sigma_1=9.0$ ,  $\mu_2=89$ ,  $\sigma_2=8.5$ ,  $\mu_3=131$ ,  $\sigma_3=7.2$ .

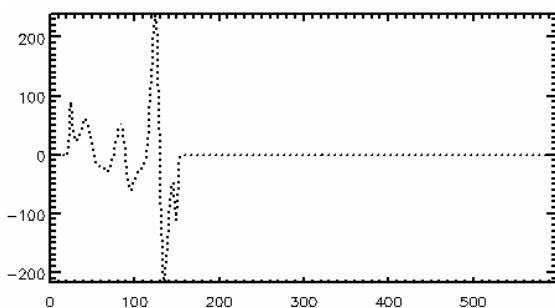


Fig.6 First derivative of waveform

Figure 9, Automated last return detection software is applied to the backscatter waveform to identify the start, peak, and end of the last return, inferred to be from the ground. In Figure 9 the laser pulse hits the canopy first and creates one echo pulses. A fraction of the laser pulse also hits the ground giving rise to a twice echo pulse. The vertical lines in the figure illustrate the positions of the ground extracted by the SLICER.

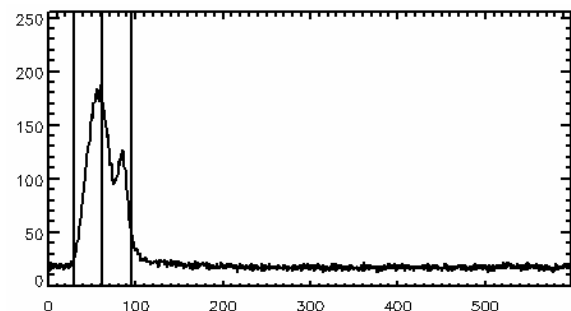


Fig.9 Ground location of SLICER

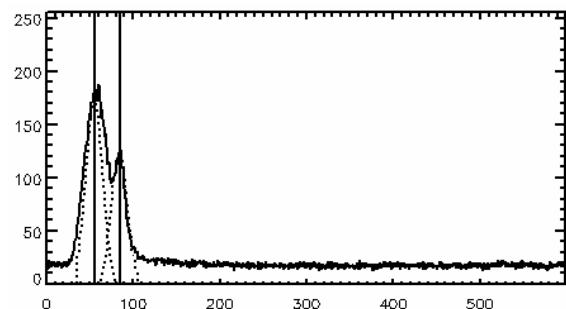


Fig.10 Simulated waveform

Figure 10. Waveform (solid) and two fitted Gauss components (dashed),  $\mu_1=57$ ,  $\sigma_1=7.3$ ,  $\mu_2=83$ ,  $\sigma_2=7.3$ . Vertical lines show the positions of the echoes extracted by the Gaussian decomposition. The EM algorithm performs well in decomposing overlapping echo pulses.

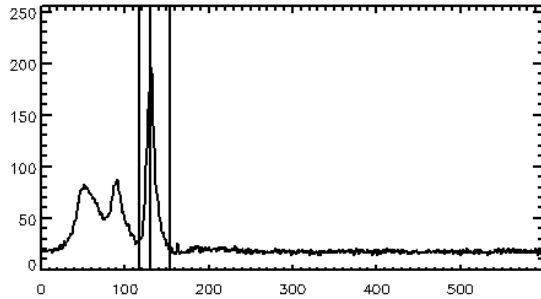


Fig.11 Ground location of SLICER

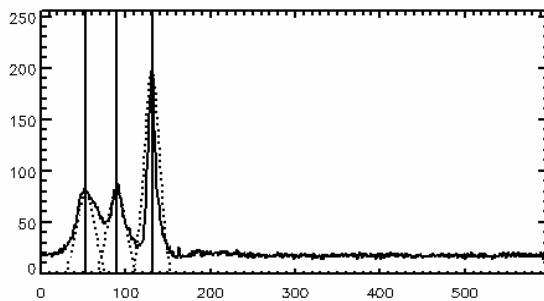


Fig.12 Simulated waveform

In Figure 11, algorithm of SLICER has detected only one peak that is ground, but three gauss components have been estimated from the waveform by Gaussian decomposition in Figure 12.

#### 4.2 RIEGL

Riegl waveform data is provided in two files, LWF files containing the calibrated waveform sample data, LGC files containing the geocoding and indexing information for each laser shot. Each waveform consists of a byte array of STRTWLEN (start waveform length) samples representing the (emitted) start pulse waveform of a laser shot for reference, followed by a byte array or ushort array of WFLLEN (waveform length) samples representing the surface return waveform. The distance from one sample to the next (1 bin) is 0.149855 m. such as Fig 13.

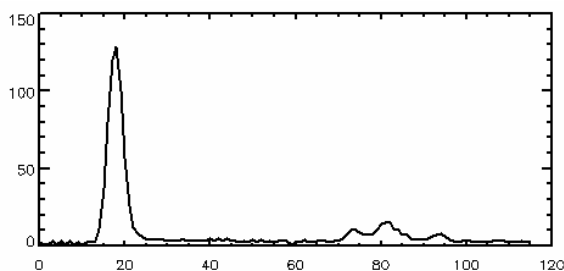


Fig.13 Unprocessed waveform of RIEGL

Due to Each waveform consists of the (emitted) start pulse waveform of a laser shot for reference. The threshold  $\sigma_{noise}$  is derived on a per shot by calculating the mean of the last 5% of the waveform record,  $\sigma_j$  is set to 1. Fig14 is Pre-processed waveform, horizontal lines show the positions of threshold  $\sigma_{noise}$ .

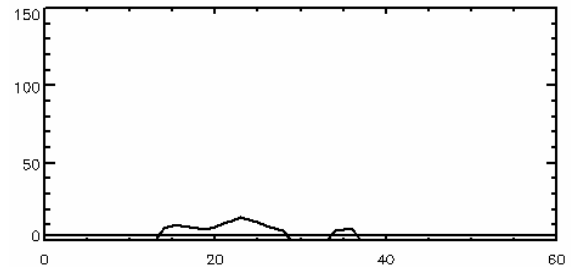


Fig.14 Pre-processed waveform

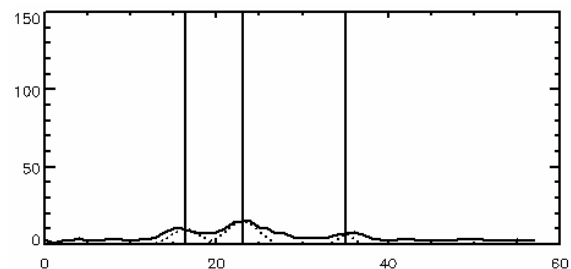


Fig.15 Simulated waveform

Three gauss components have been estimated from the waveform in Figure 15, Vertical lines show the positions of the echoes extracted by the Gaussian decomposition,  $\mu_1=16.4$ ,  $\sigma_1=1.6$ ,  $\mu_2=23$ ,  $\sigma_2=1.9$ ,  $\mu_3=35.1$ ,  $\sigma_3=0.8$ .

The performance of the system is to be compared to the performance of the EM algorithm. Table1 summarizes the performance of the two detection methods. It is obvious that post-processing of registered waveforms yield more information than the coordinates that the system outputs.

Number of echoes per waveform	Point-cloud of gaussian decomposition	Point-cloud of system	Number of additional echoes
1	2452648	2469309	-16661
2	426474	85208	+341266
3	51970	664	+51306
4	3969		+3969
5	230		+230
6	13		+13
7	1		+1
	2935305	2555181	+380124

Tab.1 comparison of the system and Gaussian decomposition

Registering the waveforms has made it possible to extract more than three echo pulse for each waveform and also to compute the width of the echoes. Pose-processing also enables detection of echoes with a smaller separation than the system does. A greater beam divergence would probably yield more multiple echo pulses since more objects would be illuminated by the same laser beam.

### 4.3 Waveform for forestry application

Lidar remote sensing has vast potential for the direct measurement and estimation of several key forest characteristics (Table 1). The direct measurements of small-footprint lidar are canopy height, subcanopy topography, and the vertical distribution of intercepted surfaces between the canopy top and the ground. Other forest structural characteristics, such as aboveground biomass, are modeled or inferred from these direct measurements

#### 4.3.1 Treeheight

With small-footprint systems, the first return above a noise threshold can be used to estimate the top of the canopy, and the midpoint of the last return represents the ground return.

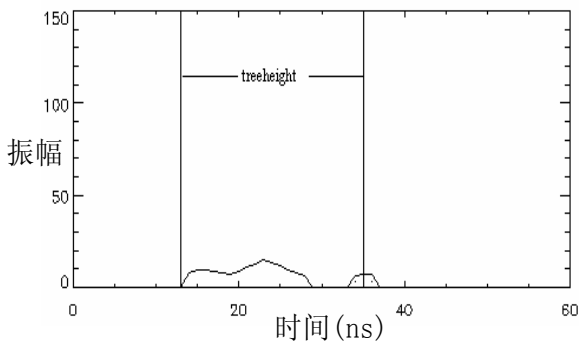


Fig16 Treeheight

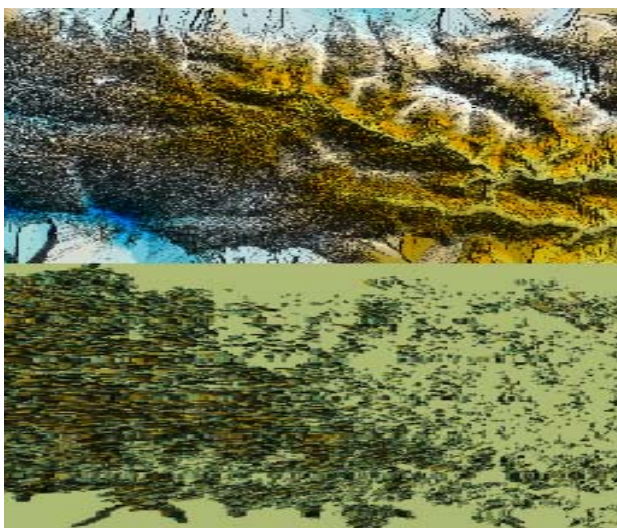


Fig17 Map of treeheight

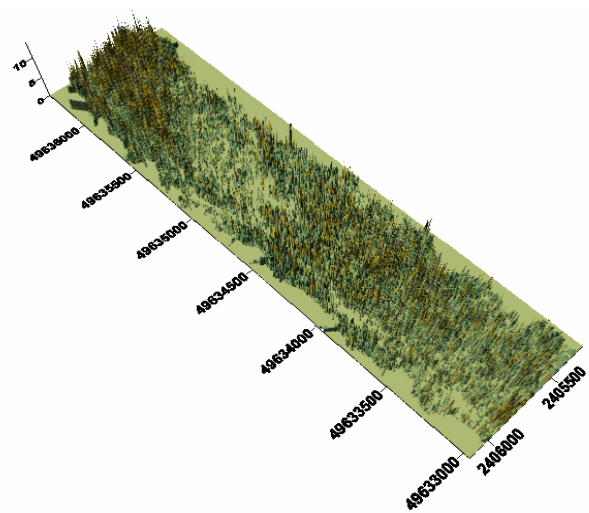


Fig18 Map of treeheight

#### 4.3.2 Crown volume

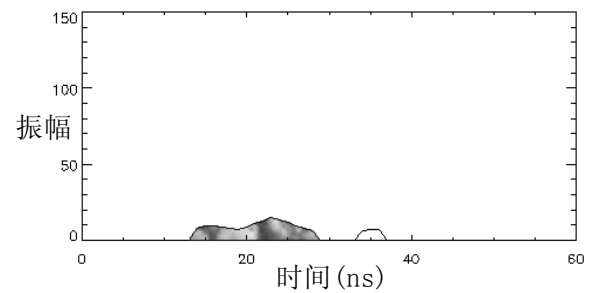


Fig19 Sketch map of Crown volume

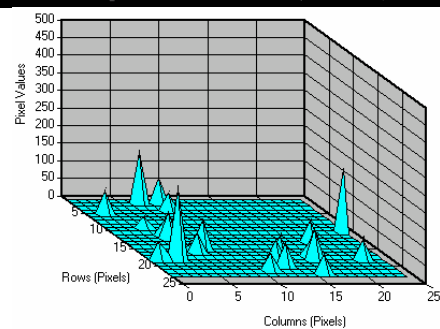
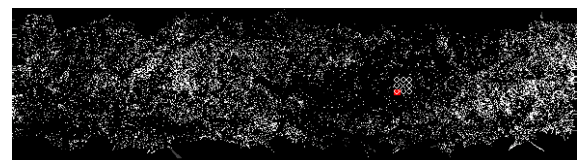


Fig20 Local Crown volume

## 5 CONCLUSION

In anticipation of the potential of full-waveform lasers for vegetation mapping experimental systems have already been built and tested by NASA. Soon, also commercial full-waveform systems have become available. It appears that full-wave systems will much enhance our capability to map natural and artificial objects, but this comes at a cost: Instead of having one or a few trigger pulses the whole discrete signal

must be stored. Major research and development efforts will be needed in order to develop algorithms and software that can efficiently transform the recorded waveform clouds into geo-spatial data sets. EM algorithm has been created to decompose a laser altimeter return waveform from simple and complex surfaces into a series of Gaussians. By analysis of the backscattered signal, it should also be possible to determine quality parameters for a given range measurement, which can be used as a direct input into further processing steps.

## REFERENCES

- Ackmann, F. Airborne laser scanning—present status and future expectations[J], *ISPRS Journal of Photogrammetry & Remote Sensing* 54\_1999.64–67
- Baltsavias, E. P: A comparison between photogrammetry and laser scanning[J], *ISPRS Journal of Photogrammetry & Remote Sensing* 54\_1999.83-94
- Bilmes J A. A Gentle Tutorial of the EM Algorithm and its Application to Parameter Estimation for Gaussian Mixture and Hidden Markov Models[C].Department of Electrical Engineering and Computer Science , U. C. Berkeley TR-97-021, April 1998
- Dempster, A. P., Laird, N. M. and Rubin, D.B., 1977.Maximum Likelihood from incomplete data via the EM algorithm[J]. *Journal of the Royal Statistical Society, Series B*,39(1),1-38
- Gamba, P., Houshmand, B.: Digital Surface Models and Building Extraction: A Comparison of IFSAR and LIDAR Data[J], *IEEE TRANSACTIONS ON GEOSCIENCE AND REMOTE SENSING, VOL. 38, NO. 4, 2000*,1959~1968
- Hofton, M. A., Blair, J. B. and Minster, J., 2000.Decomposition of Laser Altimeter Waveforms[J]. *IEEE Transactions on Geoscience and Remote Sensing*,vol.38,no 4.pp.1989-1996.
- Hyypä J, et al. Algorithms and methods of airborne laser scanning for forest measurement[C].*International Archives of Photogrammetry, Remote Sensing and Spatial Information Science*,2004,36:82-8
- Mean, J.E., Acker, S.A., Harding, D.J., Blair, J.B., Lefsky, M.A., Cohen, W.B., Harmon, M.E., and McKee, W.A. (1999), Use of large-footprint scanning airborne lidar to estimate forest stand characteristics in the Western Cascades of Oregon. *Remote Sensing of Environment* 67:298-308.
- Nilsson, M. (1996), Estimation of tree heights and stand volume using an airborne lidar system. *Remote Sens. Environ.* 56:1-7. Oliver, J. J., Baxter, R. A. and Wallace, C. S., 1996. Unsupervised Learning Using MML[C], *Machine Learning. Proceedings of the Thirteenth International Conference (ICML 96)*, Morgan Kaufmann Publishers, San Francisco CA USA, pp. 364-372
- Optech: ALTM Waveform Digitizer Operation and Processing Manual ALTM 3100[S], Oct. 2006, 66pp
- Ralph D, Robert K, Michelle H, et al. Land Surface Characterization Using Lidar Remote Sensing. In: M Hill and R Aspinall, [eds.]. *Spatial Information for Land Use Management*. International Publishers Direct, Singapore, 2000
- Ralph O D, Jason B D. Lidar Remote Sensing for Forestry Applications. *Journal of Forestry*, 2000, 98:44-46
- Wagner, W., Ullrich, A., Ducic, V., Melzer, T., Studnicka, N., 2006. Gaussian decomposition and calibration of a novel small-footprint full-waveform digitizing airborne laser scanner[J]. *ISPRS journal of Photogrammetry and Remote Sensing* 60(2), 100-112.
- Wagner, W., Ullrich, A., etc: From single-pulse to full waveform airborne laser scanners: potential and practical challenges[C], *ISPRS XXth Congress, Istanbul, Vol XXXV, Part B/3*, pp.201-206
- wehr, A, Lohr, U: Airborne laser scanning—an introduction and overview[J], *ISPRS Journal of Photogrammetry & Remote Sensing* 54\_1999.68~82

